Electrifying Industrial Wood Drying: Techno-Economic Assessment for High-Temperature Heat Pumps in Belgium

Aitor Cendoya[a], Frederic Ransy[a], Bentao Guo[a], Sylvain Quolin[a] and Vincent Lemort[a]

[a] *Thermodynamics Laboratory, Faculty of Applied Sciences, University of Liège, Liège, Belgium, acendoya@uliege.be*

Abstract:

This paper presents a techno-economic feasibility assessment of replacing a natural gas fire-tube boiler with a high-temperature heat pump (HTHP) as the primary heat source for an industrial batch wood drying kiln loaded with Norway Spruce (Picea abies) in Belgium. A thermodynamic steady-state energy and mass balance model is developed in EES to quantify the kiln heating demand across seven sequential drying stages spanning a 48-hour cycle, with dry-bulb temperatures ranging from 55°C to 100°C. The HTHP performance data is derived from a real machine with a maximum supply temperature of 130°C, ensuring that commercially available technology forms the basis of the analysis. Economic simulation is performed for the period March 2025 to March 2026 using hourly day-ahead electricity prices, daily TTF natural gas spot prices, and EU ETS CO_2 allowance costs within the Belgian regulatory framework. The total annual kiln heating demand is 1680.9 MWh, and the HTHP achieves an average annual COP of 3.67, delivering 2183.8 MWh of heat at an electricity consumption of 631.4 MWh, while the boiler requires 2459.7 MWh of natural gas (at higher heating value, PCS) for an equivalent thermal output. The HTHP achieves annual operating cost savings of €63134 (36.3% reduction) relative to the boiler, with a Levelized Cost of Heat (LCOH) of 58.2 €/MWh versus 82.1 €/MWh for the boiler, a 29.1% reduction. The cumulative net present value (NPV) payback period is approximately 3 years, with a total discounted saving of approximately €705k over a 25-year project lifetime. The results highlight that CO_2 emission charges under the EU ETS represent 25–35% of the monthly boiler operating cost, while electricity network fees and levies account for approximately 51% of the HTHP electricity bill, revealing a critical regulatory asymmetry that constrains the economic competitiveness of industrial electrification.

Keywords:

High-temperature heat pump; Wood drying kiln; Techno-economic analysis; Industrial decarbonisation.

1. Introduction

Industry is one of the most energy-intensive and carbon-emitting sectors of the global economy, largely due to its reliance on fossil fuels for process heat generation. In Europe, natural gas-fired boilers remain the dominant technology for industrial heat supply [1]. In this context, the European Union has established a comprehensive decarbonisation agenda targeting climate neutrality by 2050, supported by regulatory instruments such as the EU Emissions Trading System (EU ETS), established in 2005 and covering combustion installations above 20 MW thermal capacity, which introduces a direct financial penalty on CO_2 emissions [2], and alongside the new ETS 2 market entering in 2027, targeting industries not covered by ETS 1.

Wood drying is a representative example of an industrial thermal process that relies mainly on gas-fired boilers, involving significant thermal energy consumption across multiple drying stages and considerable annual CO_2 emissions, making it an important target for industrial decarbonisation. The use of heat pumps in drying systems is not new, since before the 2000s, heat pump dryers have been applied across various industrial contexts [3]. Despite its relevance, the electrification of conventional large-scale industrial drying kilns through high-temperature heat pumps (HTHPs) has received limited attention in the literature.

Existing studies on HP integration in wood drying processes have been reviewed comprehensively by Gao et al. [4], who highlight a persistent research gap: the lack of rigorous assessment of HP integration with conventional kilns operating under realistic temperature-humidity schedules, and no real economic metrics for comparison with fossil fuel alternatives, have been presented. In addition, recent studies have focused on

integrating of HP into the kiln [5]-6], however, both are limited to a small scale and do not include any economic comparison with the reference technology, such as gas boilers.

This paper addresses this gap by presenting a techno-economic feasibility assessment of replacing a natural gas fire-tube boiler with a high-temperature HP (HTHP) for an industrial batch wood drying kiln loaded with Norway Spruce (*Picea abies*), one of the most commercially relevant timber species in Belgium. The HTHP performance data are derived from a real machine with a maximum supply temperature of 130°C, ensuring that the results are based on commercially available technology. The economic analysis incorporates the most recent CO_2 allowance prices, gas spot prices, and day-ahead electricity market prices, together with all applicable network charges, taxes, and levies in the Belgian regulatory context, providing a rigorous and replicable framework for evaluating the economic viability of industrial heat pump deployment under current European energy market and policy conditions.

2. Methodology

2.1. Kiln Drying

The simulated kiln corresponds to a batch high-temperature kiln, operating at dry-bulb temperatures exceeding 100°C. The drying process is governed by three distinct periods. During the first and second periods, free water evaporation dominates the moisture removal mechanism. The third drying period begins once the evaporation plane has receded to the mid-plane of the board; from this point onward, bound water diffusion and water vapour flow become the controlling transport mechanisms. The drying schedule is carried out across seven sequential stages, as presented in Figure 1. In each stage, the dry-bulb temperature (T_{db}) and wet-bulb temperature (T_{wb}) are independently controlled within the kiln chamber, allowing precise regulation of the air-side Equilibrium Moisture Content (EMC). This drives the moisture gradient between the circulating air and the wood boards, progressively reducing their Moisture Content (MC) from an initial value of approximately 100% down to the target final MC (≈10%). The full drying cycle spans 48 hours, with each stage assigned a standardised duration.

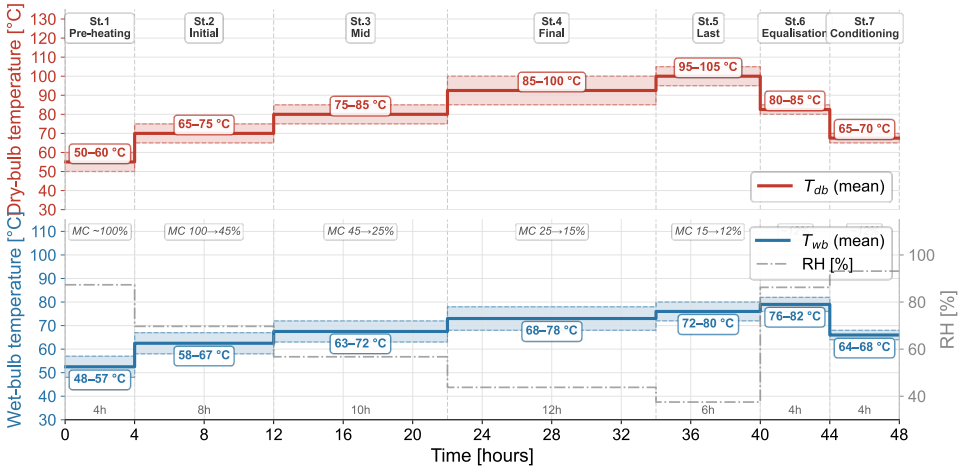

Figure. 1. *Control dry-bulb, wet-bulb temperatures and relative humidity for the Picea-Abies drying.*

A critical constraint throughout the process is the rate of moisture removal, which must remain sufficiently gradual to prevent the development of drying defects such as internal cracking and structural warping of the boards. While more aggressive schedules reduce drying time and improve economic performance, careful scheduling is essential to preserve the structural integrity and dimensional stability of the final product. The kiln configuration is presented in Figure 2, which shows the main energy flows involved in the overall energy balance. The heating system typically consists of water or steam coils that supply and maintain the dry-bulb temperature setpoint within the chamber. Moisture control is achieved through a humidifier, which regulates the wet-bulb temperature by steam injection or water atomizer, and consequently, the air-side EMC.

Air circulation is provided by variable-frequency fans, which drive the airflow across the timber stack. This forced convection simultaneously evaporates moisture from the wood boards and raises their sensible heat content. Fresh air intake and humid air exhaust are managed through damper vents and an internal recuperative heat exchanger, which are operated periodically to purge excess humidity from the chamber. Finally, uncontrolled air infiltration through the kiln envelope and heat losses through the walls, roof, and floor represent additional terms in the energy balance. In order to quantify the energy balance and the heating demand of the kiln across the seven-stage schedule, a thermodynamic steady-state energy and mass balance

model was developed in EES. The model resolves, for each stage independently, the moisture evaporation rate, the purge cycles, and the total heat demand supplied by the heating system.

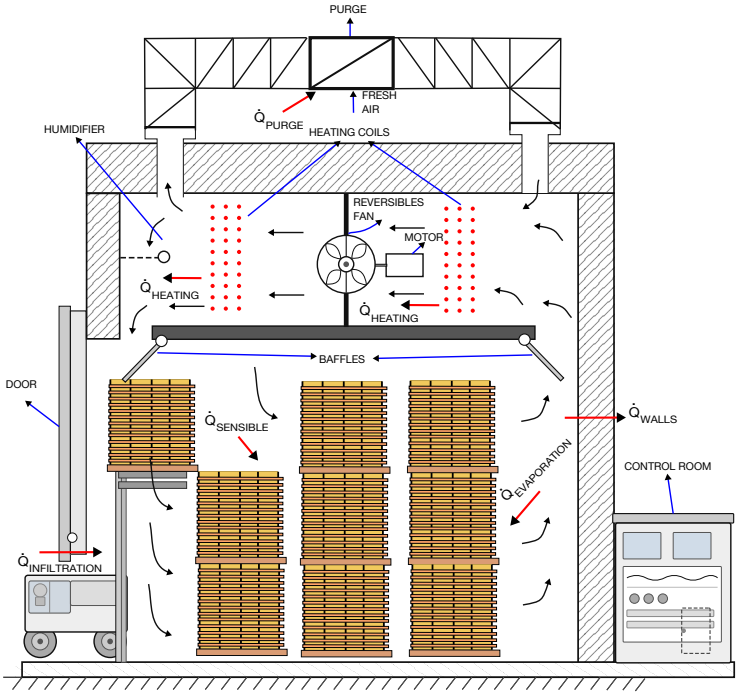

Figure. 2. *High-Temperature Batch-Kiln energy representation process.*

One of the main control variables is the EMC, which corresponds to the moisture content that wood reaches at thermodynamic equilibrium with the surrounding air, representing the asymptotic lower bound of the drying process. This equation requires empirical coefficients $K, K_1, K_2, and\ K_3$, which are functions of the dry-bulb temperature T_{db} [7].

$$EMC = \left(\frac{1800}{K_3}\right) \cdot \left(\left(\frac{K \cdot RH_{a,kiln}}{1-K \cdot RH_{a,kiln}}\right) + \frac{\left(K_1 \cdot K \cdot RH_{a,kiln} + 2 \cdot K_1 \cdot K_2 \cdot \left(K \cdot RH_{a,kiln}\right)^2\right)}{\left(1 + K_1 \cdot K \cdot RH_{a,kiln} + K_1 \cdot K_2 \cdot \left(K \cdot RH_{a,kiln}\right)^2\right)}\right) \quad (1)$$

The evaporation rate per stage is calculated from the wood moisture content at the inlet ($CH_{o,i}$) and outlet ($CH_{f,i}$) of each stage, the dry wood mass (M_{wood}), and the stage duration (τ_i), as given in Eq. (2). During stages St.1–5, evaporation is positive (drying); during St.6–7, the value is negative because the wood reabsorbs moisture from the water humidifier during the conditioning phases.

$$\dot{M}_{evap,i} = M_{wood} \cdot ((CH_{o,i} - CH_{f,i})/100)/\tau_i \quad (2)$$

To maintain the target air-side EMC within a tolerance of ±5% RH, the evaporated moisture must be continuously purged ($\dot{M}_{purge}$) from the kiln. The purge mass flow rate is determined by the difference in humidity ratio between the kiln air ($W_{a,kiln,i}$) and the ambient supply air ($W_{a,amb}$), as in Eq. (3).

$$\dot{M}_{purge,i} = \dot{M}_{evap,i} \cdot /(W_{a,kiln,i} - W_{a,amb}) \quad (3)$$

The duration of each purge cycle varies significantly across the schedule. In the early stages, where evaporation rates are highest, the dampers operate nearly continuously or at short cycle intervals (order of seconds). In the final stages, where little moisture is released, purge cycles extend to several minutes. The purge open time per cycle is given by Eq. (4).

$$\tau_{purge,i} = \frac{W_{a,kiln,i,max} - W_{a,kiln,i,min}}{\dot{M}_{evap,i}} \quad (4)$$

Energy Balance — Drying Stages (St.1–St.5)

The total heat demand rate for each drying stage is the sum of five contributions, as expressed in Eq. (5):

$$\dot{Q}_{total,i} = \dot{Q}_{evap,i} + \dot{Q}_{purge,i} + \dot{Q}_{wall,i} + \dot{Q}_{sensible,i} + \dot{Q}_{infiltration} \quad (5)$$

Air infiltration through door gaps and seals represents an additional heat loss term. An infiltration rate of 3% of the internal circulating air volume flow is assumed [9], giving Eq. (6). This small increase of the humidity into the kiln is not considered.

$$\dot{Q}_{inf,i} = \dot{V}_{a,inf,i} \cdot \rho_{a,amb} \cdot c_{p,a,amb} \cdot \left(T_{a,db,kiln,i} - T_{a,amb}\right) \quad (6)$$

The sensible load $\dot{Q}_{sensible}$ accounts for the one-time heating of the wood mass from the temperature of the previous stage to the current stage setpoint. The specific heat capacity of wood (cp_{wood}) is a function of MC, calculated as $cp_{wood} = 1.7 + 4.19 \cdot (MC/100)$, following Ref. [8], as given in Eq. (7).

$$\dot{Q}_{sensible,i} = M_{wood} \cdot cp_{wood} \cdot (T_{db,kiln,i} - T_{db,kiln,i-1}) \quad (7)$$

The wall heat losses $\dot{Q}_{walls}$ are computed using a one-dimensional steady-state U-value formulation, with an internal convective coefficient (h_{int}) of 25 W/m²K (forced convection) and an external coefficient (h_{ext}) of 15 W/m²K, as given in Eq. (8).

$$\dot{Q}_{walls,i} = \frac{1}{\frac{1}{h_{int}} + \frac{th_{kiln}}{\lambda_{iso}} + \frac{1}{h_{ext}}} \cdot A_{kiln} \cdot (T_{db,kiln,i} - T_{a,amb}) \quad (8)$$

The purge heat losses $\dot{Q}_{purge}$ represent the enthalpy difference between the hot humid kiln air exhausted and the cold dry ambient air that replaces it, as given in Eq. (9). In this equation, the term, ε_{rec} corresponds to 80% and is the recuperative efficiency of the heat exchanger for the leaving warm-wet air and the fresh air.

$$\dot{Q}_{purge,i} = \dot{M}_{purge,i} \cdot \left(h_{a,kiln,i} - h_{a,amb}\right) \cdot \varepsilon_{rec} \quad (9)$$

The evaporation heat $\dot{Q}_{evap}$ is the energy required to evaporate moisture from the wood, as given in Eq. (10).

$$\dot{Q}_{evap,i} = \dot{M}_{evap,i} \cdot h_{evap,kiln,i} \quad (10)$$

Below the Fibre Saturation Point (FSP ≈ 30%), bound water requires an additional differential heat of sorption h_s above the latent heat of free water, as expressed in Eqs. (11) and (12). Equation (12) is valid for MC < 30% [9].

$$h_{evap,kiln,i} = h_{fg,w,kiln,i} + h_{s,kiln,i} \quad (11)$$

$$h_{s,kiln,i} = 1150 \cdot \exp(-0.085 \cdot MC) \quad (12)$$

Energy Balance — Conditioning Stages (St.6–St.7)

During the conditioning stages, the wood reabsorbs moisture from the kiln air. The energy balance structure differs from that of the drying stages, as expressed in Eq. (13). In these stages, humidity is supplied by a spray system that injects atomized water or steam into the kiln chamber; the energy required to evaporate this water represents an additional heat demand on the system. The sorption heat, by contrast, corresponds to the exothermic heat released as the wood absorbs moisture, and is therefore returned to the chamber air, partially offsetting the total heat load.

$$\dot{Q}_{total,i} = \dot{Q}_{sorp,i} + \dot{Q}_{spray,i} + \dot{Q}_{wall,i} + \dot{Q}_{sensible,i} + \dot{Q}_{infiltration} \quad (13)$$

The additional terms in these stages account for the spray water injected into the kiln to raise the equilibrium moisture content (EMC). The associated heat load is given by:

$$\dot{Q}_{spray,i} = \dot{M}_{evap,i} \cdot h_{fg,w} \quad (14)$$

Since water adsorption is an exothermic process, the inverse of desorption, the heat released during moisture uptake by the wood is returned to the chamber air, thereby reducing boiler demand:

$$\dot{Q}_{sorp,i} = -\dot{M}_{evap,i} \cdot h_{s,kiln,i} \quad (15)$$

The model assumes a linear moisture distribution across all stages. Regarding damper control, when the purge interval is shorter than one minute, the vents are treated as partially open; for longer intervals, an on/off control strategy is applied.

2.2. Heating System

The heating systems are presented in Figure 3, which shows how the main heat source connects to the process and how the return flow is managed. Two alternative configurations are proposed: a fire-tube boiler operating on fossil fuels (1), and a high-temperature heat pump (HTHP-8). Both solutions are represented in the same figure, however, the installation is designed to accommodate only one of the two options, which are mutually exclusive.

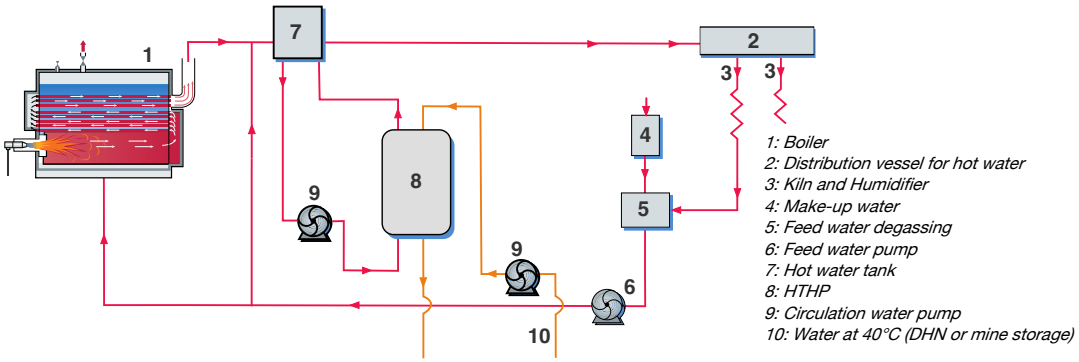

Figure. 3. *Heating system analysed, fire-tube boiler (1) and HTHP (8).*

The fire-tube boiler operates on natural gas, the fossil fuel most commonly available to industry in Belgium. The HTHP, by contrast, is electrically driven. Both systems deliver pressurised hot water, which at the same time is connected to a water tank (7) where water is controlled to a maximum value of 110°C, and the required heating capacity is determined from the kiln energy model (Section 2.1). In addition, the heating losses of the hydraulic system (piping and tank) are also considered.

In the HTHP configuration, the heat source consists of water supplied either by a district heating network (DHN) or, as in the present case, primarily from a geothermal source. This corresponds to the actual setup of this HTHP, which obtains these temperatures from abandoned mine cavities [12]. For this analysis, the heat source temperature is assumed constant (40°C). It should be noted, however, that this assumption could be further discussed in future work by replacing the geothermal source with an air-source refrigeration unit, which would supply the condensation heat directly to the evaporator of the HTHP, an extension that is identified as one of the perspectives of this study.

The thermal output of the fire-tube boiler is calculated as presented in Eq. (16), following the classical energy balance for combustion systems, where η_{boiler} is taken as 90%. In this equation, $\dot{Q}_{boiler}$ corresponds to the heating demand of the kiln, and $\dot{V}_{gas}$ is the resulting gas volumetric flow rate, which is subsequently used to calculate the gas bill.

$$\dot{Q}_{boiler} = \dot{V}_{gas} \cdot LHV_{gas} \cdot \eta_{boiler} \tag{16}$$

For the HTHP, the compressor power and the system COP_{HTHP} are presented in Figure 4, together with the operating envelope.

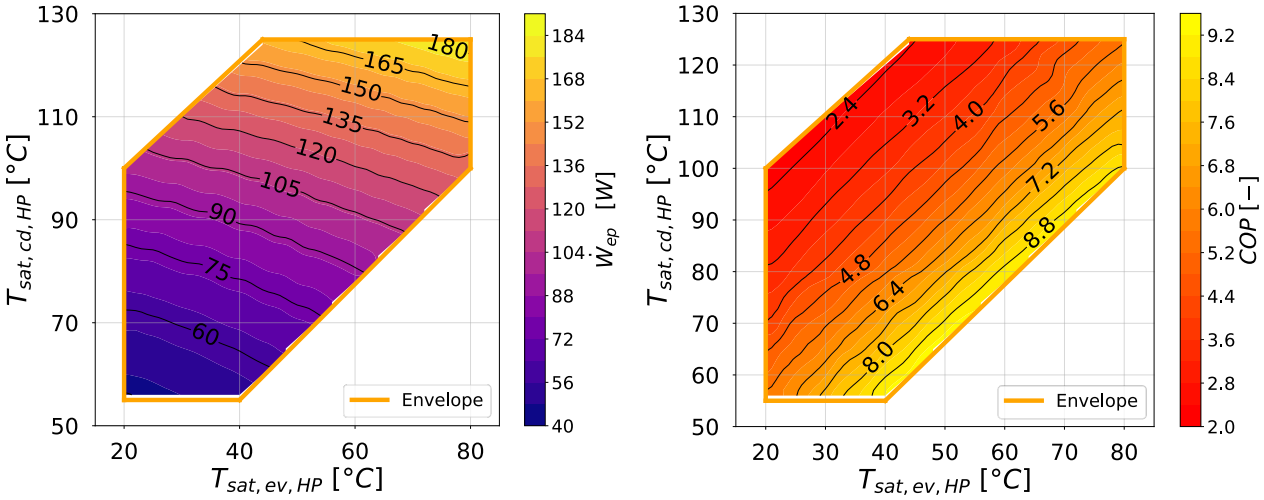

Figure. 4. *HTHP performance, left electricity consumption (compressor power), right COP performance*

A detailed description of how this envelope is obtained, including the thermodynamic methodology and the components involved, is provided in the following references [10], [11]. This machine uses R1233zd(E) as the

working fluid and incorporates a high-temperature compressor CSH2T9573 from Bitzer. It was designed to be integrated into flooded mines for long-term energy storage, with a thermal power ranging from 200 to 700 kWth, depending on operational conditions. The machine consists of two plate heat exchangers from Alfa Laval and one pneumatic expansion valve from Schubert Salzer. The heating capacity of the HTHP is calculated as presented in Equation (17), where $\dot{W}_{cp,HTHP}$ is the compressor electrical power drawn from the grid, which constitutes the electricity consumption to be costed in the economic analysis.

$$\dot{Q}_{HTHP} = \dot{W}_{cp,HTHP} \cdot COP_{HTHP} \quad (17)$$

2.3. Economic Analysis

The economic model is based on the Levelized Cost of Heat (LCOH) and the cumulative Net Present Value (NPV), calculated for both heating alternatives. For the fossil fuel option, the CAPEX considers the fire-tube boiler and burner as a package unit. For the HTHP, the full system integration is accounted for, including all associated components. The capital costs and OPEX for both systems are summarised in Table 1.

The CAPEX for the fire-tube boiler is estimated using the cost function reported by Grosse et al. (2017) [12], reference study for large-scale heating technologies in the EU, which provides a nominal investment for tank-type hot water boilers in Central Europe, and confirms a technical lifetime exceeding 25 years for the boiler body. The CAPEX for the HTHP is based on the actual component costs of a system developed within the WeForming project, in which a semi-reversible Carnot Battery (CB) was designed and built [10], [11]. The cost reported in Table 1 corresponds to the total expenditure of the HTHP cycle. This machine is currently in the commissioning phase and will be experimentally tested to validate the COP values presented in Figure 4.

Table 1. *CAPEX and OPEX costs for both solutions (400 kW HTHP and a 350 kW Fire-Tube Boiler).*

Solution	Description	CAPEX, €	OPEX, €	N (year)
HTHP	Compressor, heat exchangers, valves, power electronics, piping, insulation, installation, sensors, structure, personal months	196869	1.5% CAPEX	25
	Electricity	-	$C_{a,HTHP} = \sum\left(\left(c_{grid} + c_{fee}\right) \cdot E_{a,HTHP}\right)$	-
Boiler	Fired-tube boiler, Burner	44100.0	1.5% CAPEX	25
	Gas	-	$C_{a,gas} = \sum\left(\left(c_{gas} + c_{co_2} + c_{fee}\right) \cdot (\dot{V}_{gas} \cdot HHV)\right)$	-

On the operating cost side, the gas price includes not only the fuel cost but also the CO_2 emission charge per ton emitted under the EU ETS-2, which increases the effective cost of the fossil fuel option. The invoiced gas energy is calculated based on the consumed gas volume multiplied by the Higher Heating Value (HHV) [13], as it is standard practice for natural gas billing in Belgium. For the HTHP, the purchased energy corresponds directly to the electrical demand of the compressor. The electricity cost incorporates the grid distribution and transport fee.

The LCOH is calculated as presented in Equation (18), applying a discount rate (i) of 5%. The denominator corresponds to the total heat delivered annually by each system. The annual energy cost term $E_{a,i}$ refers to the energy purchased from the energy carrier (gas or electricity).

$$LCOH_i = \frac{CAPEX_i + \sum_{t=1}^{N} \frac{OPEX + E_{a,i}}{(1+i)^t}}{\sum_{t=1}^{N} \frac{Q_{th,i}}{(1+i)^t}} \quad (18)$$

The cumulative NPV is calculated as presented in Equation (19), where the CAPEX difference corresponds to the additional capital investment of the HTHP relative to the boiler, and the OPEX reference represents the annual operating cost saving achieved by the HTHP in the year.

$$NPV(N) = -(CAPEX_{HTHP} - CAPEX_{boiler}) + \sum_{t=1}^{N} \frac{OPEX_{Boiler} - OPEX_{HTHP}}{(1+r)^t} \quad (19)$$

Electricity, Gas and CO_2 Prices

The energy prices used in this analysis correspond to the period 20/03/2025–20/03/2026. A multi-year simulation is not considered, as energy prices, particularly electricity, fluctuate rapidly. Natural gas prices are additionally subject to significant volatility driven by geopolitical events, as evidenced by the European energy crisis of 2022 and the 2026 crisis.

For electricity, the day-ahead or intraday market prices are used as simulation input, extracted from the ENTSO-E Transparency Platform with an hourly resolution (c_{grid}) [14]. For natural gas, the daily spot price (c_{gas}) from the TTF (Title Transfer Facility) market, reported by the Intercontinental Exchange, is adopted [15]. The TTF price is assumed to be constant on each simulation day.

In addition to the direct energy costs, two ancillary charges are accounted for. For natural gas, a CO_2 emission cost (c_{co_2}) is included, estimated according to the EU ETS 2 carbon price, assumed equal to the current EU ETS 1 market price [16]. The specific emission factor for heat generation from natural gas is 0.202 tCO_2/MWh, and an additional fee cost of the distributor of (~0.0026 €/kWh), from the taxes (~0.0121 €/kWh) and renewable levy (~0.0015 €/kWh), reaching a total network surcharge of 0.016 €/kWh (c_{fee}) [17].

For electricity, grid distribution and transport fees apply in addition to the market price. The total network fee (c_{fee}) is decomposed as follows: Transmission tariff (~0.024 €/kWh), distribution tariff (~0.026 €/kWh), and other levies (~0.0396 €/kWh), yielding a total network surcharge of approximately 0.0896 €/kWh. The distribution tariff corresponds to the average observed distribution cost for professional electricity consumers in Wallonia [18].

3. Results

The simulation was carried out over the previously mentioned period, considering a repetitive 48-hour drying cycle. The kiln modelling parameters are summarised in Table 2, and the results obtained from the assessment are discussed in the following subsections. The system parameters were selected based on the actual size of the constructed HP, ensuring that the economic comparison reflects real component costs rather than theoretical estimates. Additionally, an 80 m³ water tank is included in the system, sized to cover the peak heating demand periods.

Table 2. Parameters considered in the Kiln energy evaluation.

Parameters	Value
Wood charge [m^3]	100
Wood type, [-]	Norway Spruce (Picea abies)
Wood density [kg m^{-3}]	450
Board thickness, [mm]	25
Air circulation, [m3/h]	28000
Wall thickness, [mm]	100
Wall heat transfer, [$Wm^{-2}K^{-1}$]	0.384
Exterior Temperature, [°C]	5
Exterior humidity, [%]	80
Total envelope area, [m^2]	365.4
Free air volume, [m^3]	288.8

3.1. Kiln thermal analysis

The resulting heating demand for each drying stage, together with the purge cycle behaviour, is presented in Figure 5. The heating demand profile shows a pronounced peak during the first two stages, driven by the large temperature differential and high initial MC of the wood, followed by a substantial decrease in the intermediate stages and very low demand in the final stage. This trend reflects the progressive reduction in evaporation rate as the wood approaches its target MC. The annual kiln heating demand corresponds to 1680.9 MWh, with a heating required of 9235.5 kWh per drying cycle.

Regarding the purge cycles, three distinct operating regimes are observed. In stages 1 to 3, the moisture evaporation rate is sufficiently high that the dampers reach saturation in intervals below one minute;

consequently, they are maintained in a normally open position. In stages 4 and 5, the moisture load is lower, and the dampers operate in an on/off mode, opening periodically to discharge the required volume of humid air. In the final two stages, corresponding to the equalisation and conditioning phases, no purge is considered.

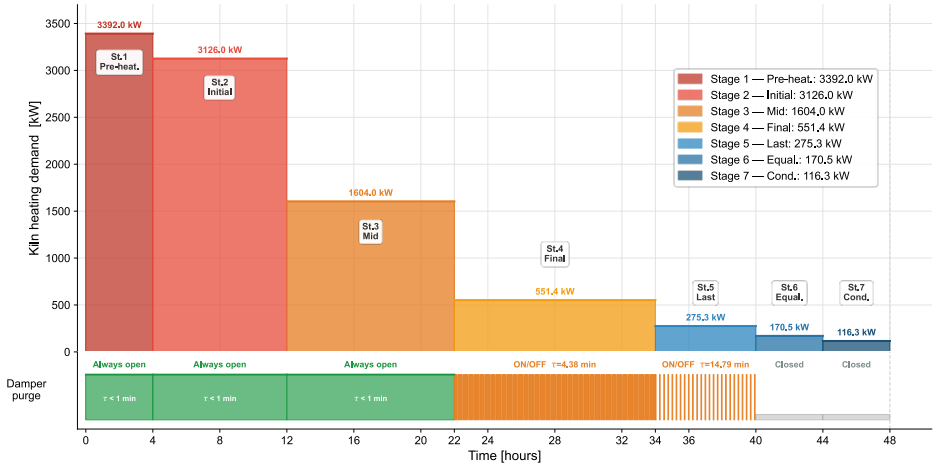

Figure. 5. *Kiln heating demand and purge opening cycles.*

In the present assessment, this limitation is addressed by assuming the availability of a 40°C water source, representative of a DHN, a mine storage or a first-stage air-to-water HP, which acts as the evaporator heat source for the HTHP and increases the operating COP. It should be noted that replacing this source with a dedicated booster HP would be a viable alternative, although it would result in higher CAPEX for the system.

3.2. Operational Performance

The operational performance of both heating systems over a representative 48-hour drying cycle is presented in Figures 6a and 6b. For the HTHP configuration, the T_{tank} tracks the required supply temperature ($T_{required}$) across all 7 drying stages, with the HTHP delivering a condenser output $\dot{Q}_{cd,HTHP}$ that partially covers the kiln demand in each stage. The COP varies throughout the cycle, reaching a peak of approximately 5.0 during the intermediate stages, where the temperature lift is lower, and decreasing to approximately 2.5 in the final stages. The HTHP is switched off during the last two stages, when the kiln operates in conditioning mode. The average COP over the full annual simulation is 3.67, with a total annual compressor electricity consumption of 631.4 MWh and a total thermal power of 2183.8 MWh.

For the boiler configuration, the system operates controlled by the T_{tank}, with the boiler firing at its nominal capacity of 350 kW whenever T_{tank} drops below 110°C. This results in a characteristic cycling pattern that becomes more frequent in the intermediate and later stages as the heating demand decreases. The annual boiler thermal output is 2213.8 MWh, corresponding to a fuel consumption of 2459.7 MWh (HHV). The small difference between the heating supplied by the HP and the boiler corresponds to heat losses, which increase due to the higher-temperature operation.

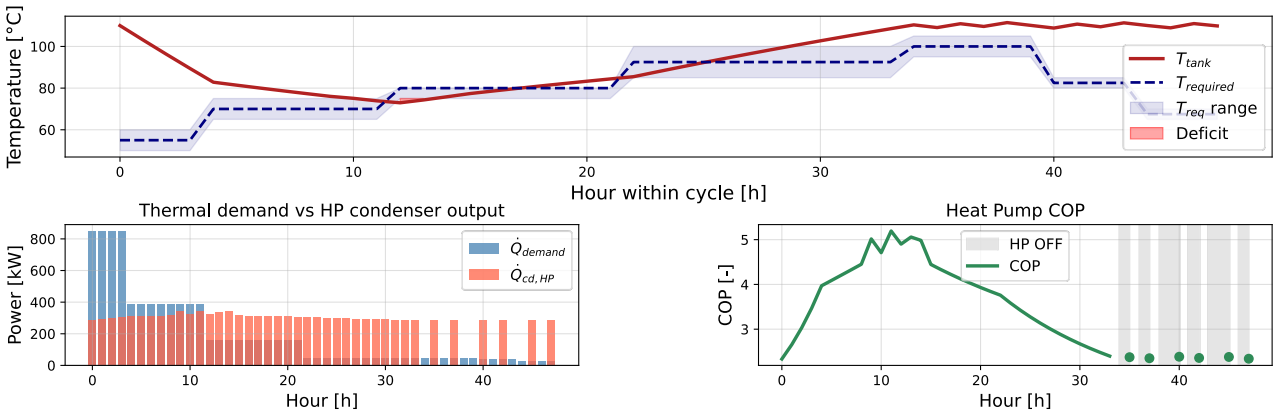

a)

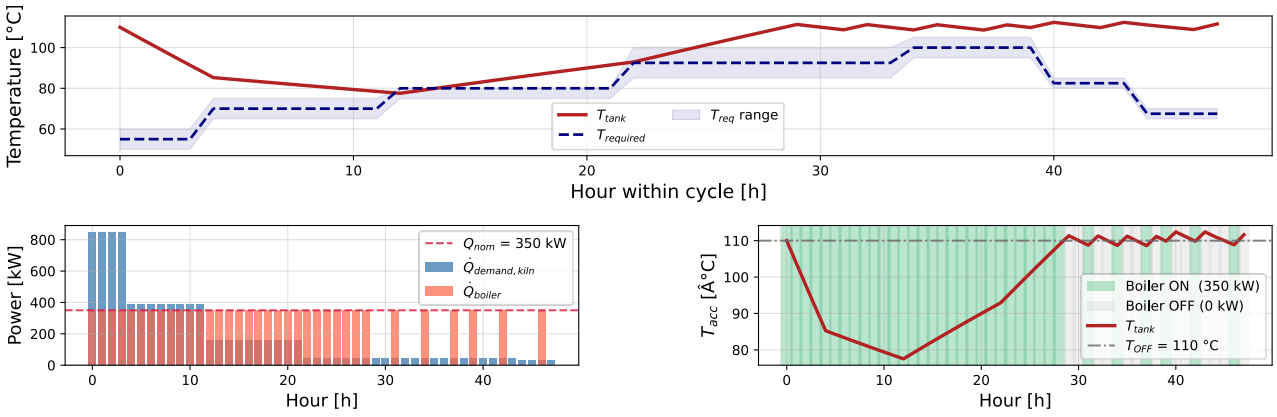

(b)

Figure. 6. HTHP (a) and boiler (b) operation for the Kiln demand.

It is important to note that the thermal deficit observed in Figure 6, where the tank temperature falls below the upper control setpoint, does not imply that the heating demand cannot be met. The system is designed with a temperature band rather than a fixed setpoint, as long as the tank temperature remains within the defined operating range, the heat delivered to the kiln is sufficient to cover the process demand at each stage.

3.3. Energy Cost Analysis

The monthly operating costs for both systems over the simulation period are presented in Figure 7. The boiler cost is consistently higher than the HTHP cost in every month of the simulation period. The boiler cost breakdown (Figure 7b) shows that CO_2 allowances represent a non-negligible fraction of the total gas cost, confirming that the carbon surcharge is a significant economic penalty for the fossil fuel option. In the case of HTHP, the predominant cost component fluctuates between TSO/DSO fees and the actual price of electricity; in some months, the charges included in the rates exceed the price of electricity, which represents a cost that can be easily adjusted through public policy.

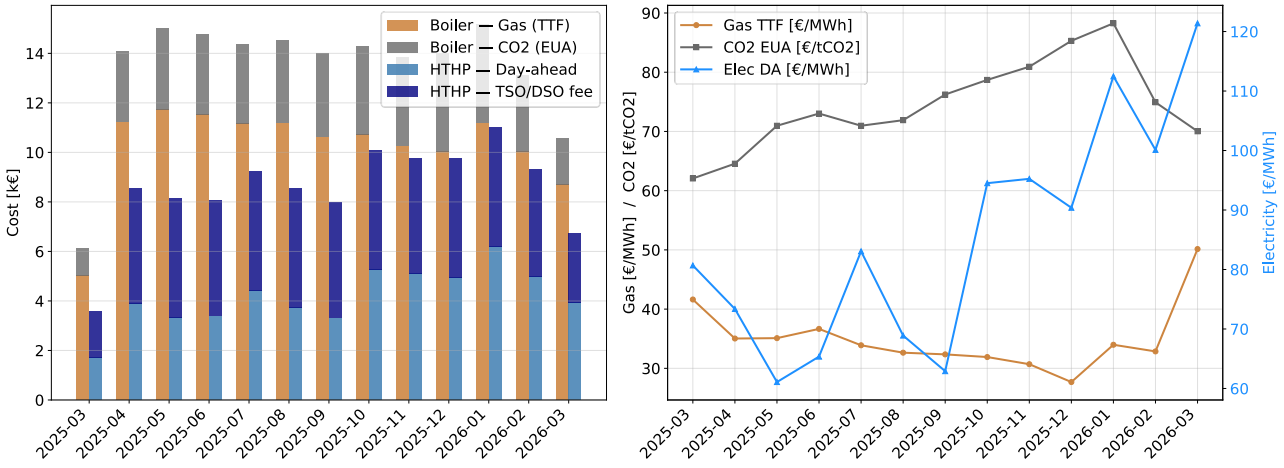

(a) (b)

Figure. 7. Monthly cost comparison, (a) energy cost breakdown, (b) average market prices.

The cumulative energy cost over the full simulation period confirms the consistent operational advantage of the HTHP: the boiler accumulates €173936 in annual operating costs, compared to €110802 for the HTHP, yielding annual savings of €63134, a 36.3% reduction in OPEX. It is worth noting that the CO_2 emission charge represents 25–35% of the total monthly boiler cost, constituting a non-negligible and structurally growing penalty for the fossil fuel option. In contrast, for the HTHP, the TSO/DSO and network fees account for approximately 51% of the total electricity bill.

In terms of unit heat cost, the boiler delivers thermal energy at 72.29 €/MWh, while the HTHP consumes electricity at 175.5 €/MWh, however, given the average COP of 3.67, the effective cost per unit of heat delivered

by the HTHP is significantly lower. It is further worth noting that the electricity unit cost is heavily influenced by network fees and levies charged by third parties. If these surcharges were reduced to a level equivalent to those applied to gas distribution, the economic advantage of the HTHP would widen considerably, increasing the operational cost gap to 63% and reducing the effective electricity cost to 101.9 €/MWh.

3.4. LCOH and NPV Analysis

The LCOH and cumulative NPV over a 25-year project lifetime are presented in Figures 8a and 8b, respectively. The LCOH breakdown shows that for the HTHP, the energy cost component dominates at 50.5 €/MWh, while the annualised CAPEX and maintenance contribute 6.4 and 1.3 €/MWh, respectively, yielding a total LCOH of 58.2 €/MWh.

For the boiler, the energy cost accounts for 80.3 €/MWh out of a total LCOH of 82.1 €/MWh, with CAPEX and maintenance being negligible by comparison. This value exceeds the annual unit heat cost because the LCOH is referred to the useful heat delivered to the system, whereas part of the fuel energy is lost through boiler inefficiency. The HTHP therefore achieves a 29.1% reduction in LCOH relative to the boiler, corresponding to a differential of 23.9. €/MWh.

The cumulative NPV analysis shows that the higher initial investment of the HTHP is recovered within approximately 3 years, after which the HTHP generates sustained savings relative to the boiler. Over the full 25-year lifetime, the total discounted cost of the HTHP amounts to approximately €1800k, compared to €2505k for the boiler, representing a total NPV saving of approximately €705k.

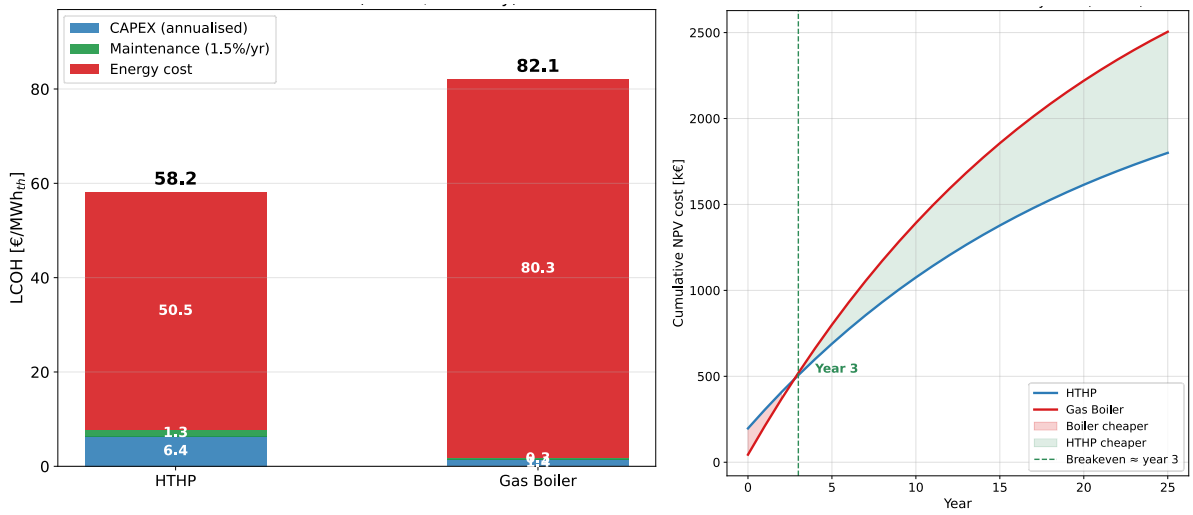

(a) (b)

Figure. 8. Economic comparison (a) LCOH, (b) cumulative NPV.

4. Conclusion & Perspectives

This study presented a techno-economic comparison between a natural gas fire-tube boiler and a HTHP as heating alternatives for an industrial batch wood drying kiln loaded with Norway Spruce with a capacity of 100 m³. The full drying schedule, comprising seven stages from 55°C to 100°C, was modelled, and the resulting heating demand was used as input to an economic simulation covering the period from March 2025 to March 2026. From the operational analysis, the HTHP achieves an average annual COP of 3.67, delivering 2183.8 MWh of heat to the kiln at an electricity consumption of 631.4 MWh. The boiler covers the same heating demand with a fuel consumption of 2459.7 MWh (HHV).

From the economic analysis, the HTHP achieves annual OPEX savings of €63134, a 36.3% reduction relative to the boiler. The boiler operating cost is significantly penalised by the CO_2 emission charge under the EU ETS, which represents approximately 25–35% of the total monthly gas cost and cannot be neglected in the economic assessment, which is also to be expected as the energy sector approaches net-zero energy targets. On the other hand, the HTHP is heavily penalised by TSO/DSO network fees and levies, which account for

approximately half of the total electricity bill paid by the end consumer. This represents a key structural barrier to industrial electrification. This finding underlines that regulatory and tariff policy reform is as important as technology development in accelerating the transition to electrified industrial heat.

The LCOH of the HTHP is 58.2 €/MWh, compared to 82.1 €/MWh for the boiler, a reduction of 29.1%. On the other hand, the NPV breakeven between HTHP and boiler is approximately 3 years, and the total saving over a 25-year lifetime amounts to approximately €705k.

In summary, HTHP represents a technically viable and economically superior alternative to natural gas boilers for industrial wood drying in Belgium. The combination of high operational efficiency, better economic metrics, and the growing impact of CO_2 costs on fossil fuels makes electrification via HTHP financially attractive.

Future work should address the integration of a booster heat pump configuration to eliminate the dependency on an external 40°C heat source, the experimental validation of the HTHP COP under real kiln operating conditions using the WeForming Carnot Battery system currently in commissioning. From an economic optimisation perspective, the sizing of the hot-water buffer tank should be further investigated to maximise the benefit of dynamic electricity pricing. Additionally, alternative operational strategies should be explored, such as operating multiple kilns of smaller individual volume in parallel, which would provide a more continuous and stable heat demand profile throughout the operating period. Finally, a sensitivity analysis with respect to future electricity and gas price trajectories under different EU energy policy scenarios would strengthen the long-term business case for industrial HTHP deployment.

Acknowledgments

The project that produced the results presented in this paper has received funding from the European Union's Horizon Research and Innovation programme under grant agreement No. 10112355, in the framework of the WeForming project. The authors would also like to acknowledge the funding provided by the Walloon Region of Belgium in the framework of the ARDNrgy project.

Nomenclature

A	area, m²	$\dot{M}$	mass flow rate, kg/s
c	cost, €/kWh	MC	moisture content, %
C	annual cost, €/year	N	lifetime, years
$CAPEX$	capital expenditure, €	NPV	net present value, €
COP	coefficient of performance, –	$OPEX$	annual operating expenditure, €/year
cp	specific heat capacity, kJ/(kg K)	LHV	lower heating value, kWh/m³
CH	moisture content, %	HHV	higher heating value, kWh/m³
E_a	annual energy consumption, MWh/year	$\dot{Q}$	heating flow rate, kW
EMC	equilibrium moisture content, %	RH	relative humidity, %
h	specific enthalpy, kJ/kg, heat transfer coefficient, W/(m² K)	T	temperature, °C
i	discount rate and operation stage, –	t	time, years
K	empirical coefficients, –	W	humidity ratio, kg_w/kg_air
$LCOH$	levelized cost of heat, €/MWh	$\dot{V}$	volumetric flow rate, m³/s
M	mass, kg	$\dot{W}$	Electrical power, kW

Greek symbols

η	efficiency	ρ	density, kg/m³
ε	effectiveness	τ	stage duration/time, h
λ	thermal conductivity, W/(m K)		

Subscripts and superscripts

a	air	rec	recuperator
amb	ambient	s	sorption
$boiler$	fire-tube boiler	sat	saturation

cd	condenser	$sensible$	sensible heat
cp	compressor	$tank$	hot water storage tank
db	dry-bulb	$total$	total
$evap$	evaporation	w	water
fg	Phase change	$wall$	kiln envelope walls
$HTHP$	high-temperature heat pump	wb	wet-bulb
inf	infiltration	$wood$	wood
$kiln$	kiln chamber		

References

[1] Eurostat, “Electricity and gas: 64.5% of industrial final energy use in 2022.” May 2024. [Online]. Available: https://ec.europa.eu/eurostat/web/products-eurostat-news/w/ddn-20240513-1

[2] European Parliament and Council of the European Union, “Directive (EU) 2023/959 amending Directive 2003/87/EC — EU ETS revision (Fit for 55).” May 2023. [Online]. Available: https://eur-lex.europa.eu/legal-content/EN/TXT/?uri=CELEX:32023L0959

[3] V. Minea, “Drying heat pumps – Part II: Agro-food, biological and wood products,” *Int. J. Refrig.*, vol. 36, no. 3, pp. 659–673, May 2013, doi: 10.1016/j.ijrefrig.2012.11.026.

[4] L. Gao *et al.*, “A comprehensive review of heat pump wood drying technologies,” *Energy*, vol. 311, p. 133241, Dec. 2024, doi: 10.1016/j.energy.2024.133241.

[5] B. Hu *et al.*, “Experimental study on a direct steam generation unit of high temperature air source heat pump,” *Energy*, vol. 330, p. 136886, Sep. 2025, doi: 10.1016/j.energy.2025.136886.

[6] M. Yao *et al.*, “Thermodynamic characteristics of a wide temperature range CO2 heat pump drying system with multistage heat recovery under low temperature conditions,” *Appl. Therm. Eng.*, vol. 289, p. 129817, Mar. 2026, doi: 10.1016/j.applthermaleng.2026.129817.

[7] W. T. Simpson, “Predicting Equilibrium Moisture Content of Wood by the Hailwood-Horrobin Theory,” U.S. Department of Agriculture, Forest Service, Forest Products Laboratory, Madison, WI, FPL-GTR-282, 1971. [Online]. Available: https://www.fpl.fs.usda.gov/documnts/fplgtr/fpl_gtr229.pdf

[8] Forest Products Laboratory, “Wood Handbook: Wood as an Engineering Material,” USDA Forest Service, Forest Products Laboratory, Madison, WI, FPL-GTR-282, 2021. [Online]. Available: https://www.fpl.fs.usda.gov/documnts/fplgtr/fplgtr282/front_matter_fpl_gtr282.pdf

[9] J. F. Siau, *Transport Processes in Wood*, vol. 2. in Springer Series in Wood Science, vol. 2. Berlin, Heidelberg: Springer Berlin Heidelberg, 1984. doi: 10.1007/978-3-642-69213-0.

[10] A. Cendoya, F. Ransy, B. Guo, A. Hernandez, O. Dumont, and V. Lemort, “Design and modelling of a reversible HP/ORC Carnot battery tailored for waste heat integration in flooded mines,” *Appl. Energy*, vol. 404, p. 127127, Feb. 2026, doi: 10.1016/j.apenergy.2025.127127.

[11] A. Cendoya, F. Ransy, O. Dumont, B. Guo, and V. Lemort, “Design, Component Selection and Critical Considerations for the Development of a 50 kWe Carnot Battery Coupled to Waste Heat,” in *Proceedings of the 8th International Seminar on ORC Power Systems (ORC 2025)*, T. Turunen-Saaresti, F. Crespi, A. Spinelli, A. Uusitalo, and M. T. White, Eds., Lappeenranta, Finland: LUT Scientific and Expertise Publications, 2025, pp. 1–10. [Online]. Available: https://lutpub.lut.fi/handle/10024/170511

[12] R. Grosse, B. Cox, C. Нчас, P. Pinero, and S. Canu, “Long-term (2050) Projections of Techno-economic Performance of Large-scale Heating and Cooling in the EU,” European Commission, Joint Research Centre, Luxembourg, JRC Technical Report JRC109006, 2017. doi: 10.2760/24422.

[13] Commission de Régulation de l’Électricité et du Gaz (CREG), “Conversion du m^3 de gaz en kWh.” [Online]. Available: https://www.creg.be/fr/a-z-index/conversion-du-m3-de-gaz-en-kwh

[14] ENTSO-E, “Transparency Platform — Day-Ahead Prices.” 2025. [Online]. Available: https://transparency.entsoe.eu

[15] Intercontinental Exchange (ICE), “TTF Natural Gas Day-Ahead Price.” 2025. [Online]. Available: https://www.ice.com

[16] European Energy Exchange (EEX), “EU ETS Carbon Allowances (EUA) Spot Price.” 2025. [Online]. Available: https://www.eex.com

[17] Eurostat, “Gas prices components for non-household consumers - annual data.” Eurostat, 2022. doi: 10.2908/NRG_PC_203_C.

[18] Commission Wallonne pour l’Énergie (CWaPE), “Analyse des prix de l’électricité et du gaz naturel en Wallonie (clients professionnels) sur la période de janvier 2009 à décembre 2024,” CWaPE, CD-25f26-CWaPE-0113, Jun. 2025. [Online]. Available: https://www.cwape.be/sites/default/files/cwape-documents/Observatoire%20des%20prix%20aux%20clients%20professionnels%20janvier%202009%20%C3%A0%20d%C3%A9cembre%202024.pdf